

# Self-induced transparency in warm and strongly interacting Rydberg gases

Zhengyang Bai<sup>1,2</sup>, Charles S. Adams<sup>3</sup>, Guoxiang Huang<sup>2</sup> and Weibin Li<sup>1</sup>

<sup>1</sup>*School of Physics and Astronomy, and Centre for the Mathematics and Theoretical Physics of Quantum Non-equilibrium Systems, University of Nottingham, Nottingham, NG7 2RD, UK*

<sup>2</sup>*State Key Laboratory of Precision Spectroscopy, East China Normal University, Shanghai 200062, China*

<sup>3</sup>*Joint Quantum Centre (JQC) DurhamNewcastle, Department of Physics, Durham University, South Road, Durham, DH1 3LE, United Kingdom*

We study dispersive optical nonlinearities of short laser pulses propagating in high number density, warm atomic vapors where the laser resonantly excites atoms to Rydberg  $P$ -states via a single-photon transition. Three different regimes of the light-atom interaction, dominated by either Doppler broadening, Rydberg atom interactions, or decay due to thermal collisions between groundstate and Rydberg atoms, are described. We show that using fast Rabi flopping and strong Rydberg atom interactions, both in the order of gigahertz, can overcome the Doppler effect as well as collisional decay, leading to a sizable dispersive optical nonlinearity on nanosecond timescales. In this regime, self-induced transparency (SIT) emerges when areas of the nanosecond pulse are determined primarily by the Rydberg atom interaction, rather than the area theorem of interaction-free SIT. We identify, both numerically and analytically, the required areas to achieve Rydberg-SIT. Our study contributes to efforts in achieving quantum information processing using glass cell technologies.

**Introduction.**— Strong and long-range interactions between atoms excited in high-lying Rydberg states [1–3] can be mapped onto weak light fields via electromagnetically induced transparency (EIT) [4–10], permitting interaction-mediate optical nonlinearities [11–17] and optical quantum information processing [18–27]. In the EIT approach, ultracold temperatures ( $\sim \mu\text{K}$ ) is of critical importance to maintain the weak dispersive nonlinearity (typically sub-megahertz). As Doppler broadening ( $\propto \sqrt{T}$  with  $T$  the temperature) increases from about 100 kilohertz at  $1 \mu\text{K}$  to gigahertz at 300 K, large thermal fluctuations at high temperatures can easily smear out the nonlinearity [28–31]. To overcome this limitation, recent experiments employ short (nanoseconds) and strong (gigahertz Rabi frequencies) lasers to excite high density, room-temperature (or hot) Rydberg gases [29, 30, 32] confined in glass cells [33–36]. Through a four-wave mixing process, strong dispersive nonlinearities even exceed the laser strength and thermal effect such that a single photon can be generated in the glass cell setting [32]. Though rapid experimental developments [29, 30, 32], theoretical understanding of the optical nonlinearity mediated by Rydberg interactions that emerges at nanosecond timescale and room temperature gases remains unavailable.

In this work we theoretically investigate dispersive optical nonlinearities of short light pulses generated in thermal gases of Rydberg atoms excited via a single-photon transition. A crucial requirement to generate strong Rydberg interactions is the high number density of the gas. Inelastic collisions between groundstate atoms and Rydberg electrons become inevitable, causing decay of the Rydberg state. Using nanosecond pulses, we identify the dispersive nonlinear regime where the Rydberg interaction surpasses the thermal and collisional

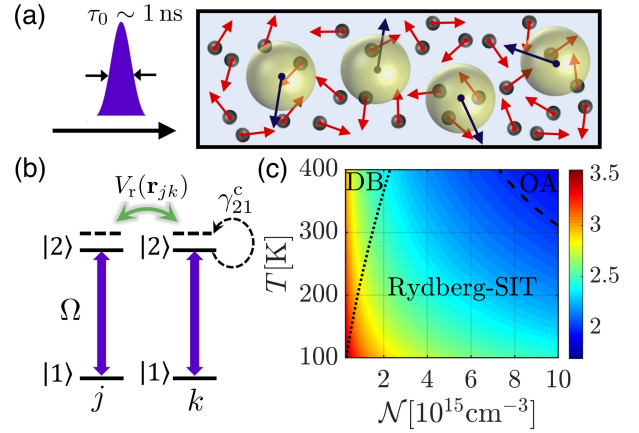


FIG. 1. (Color online) **Light-atom interactions in thermal gases.** (a) Nanosecond pulses excite thermal atoms to Rydberg states. This process is affected by thermal motions, Rydberg atom interactions, and inelastic collisions between groundstate (black dots) and Rydberg (yellow balls) atoms. (b) Level scheme. The laser (Rabi frequency  $\Omega$ ) resonantly couples groundstate  $|1\rangle$  and Rydberg state  $|2\rangle$ . The latter experiences strong, long-range van der Waals interactions  $V_r(\mathbf{r}_{jk})$  and collisional decay (rate  $\gamma_{21}^c$ ). (c) Three phases that are governed by the Doppler broadening (DB), Rydberg interactions, or optical absorption (OA) as a function of temperature and atomic density. The color bar shows the ratio of the sum of the Rydberg interaction and Doppler broadening over the collisional decay rate. In the Rydberg-SIT region, stability of the pulse is controlled by the Rydberg interaction. See text for details.

effects. Importantly this Rydberg nonlinearity depends non-perturbatively on the transient dynamics of Rydberg atoms. A key finding in this regime is that Rydberg self-induced transparency (SIT) can emerge in low and high temperature gases, where the pulse reshapes spontaneously into a bright soliton. Through numerical and mean-field calculations, we reveal explicitly the relation-

ship between the stable of Rydberg-SIT regime and the Rydberg interaction. This relationship is fundamentally different from conventional (i.e. no two-body interactions) SIT which is governed by the area theorem [37]. Our study opens opportunities to investigate Rydberg nonlinear optics and possibly to implement optical quantum information processing with warm Rydberg gases at nanosecond timescales.

**Light-atom interaction.**— We consider nanosecond laser pulses (wave vector  $\mathbf{k}$  along the  $z$  axis) propagate in a high density gas (density  $\mathcal{N}$ ), as depicted in Fig. 1a. The laser resonantly couples groundstate  $|1\rangle$  to Rydberg  $nP$  state  $|2\rangle$  (with  $n$  the principal quantum number) via a single-photon transition (see Fig. 1b). Two Rydberg atoms (located at  $\mathbf{r}_j$  and  $\mathbf{r}_k$ ) interact via the van der Waals (vdW) interaction  $V_r(\mathbf{r}_{jk}) = -C_6/|\mathbf{r}_{jk}|^6$  with  $\mathbf{r}_{jk} = \mathbf{r}_j - \mathbf{r}_k$  and  $C_6 \propto n^{11}$  to be the dispersion coefficient. In this setting, Rydberg electrons frequently collide with surrounding groundstate atoms through the polarization interaction. Using the Fermi pseudo-potential and neglecting higher order contributions [38], such interaction is approximated to be  $V_p(\mathbf{r}_{jk}) \approx 2\pi a_s \delta(\mathbf{r}_{jk})$  [39] where  $a_s$  is the s-wave scattering length of the electron-atom collision[40]. This yields the  $N$ -atom Hamiltonian ( $\hbar \equiv 1$ )

$$\hat{H} = \sum_{j=1}^N H_j + \sum_{k \neq j}^N \left[ \frac{V_r(\mathbf{r}_{jk})}{2} \hat{\sigma}_{22}^j \hat{\sigma}_{22}^k + V_p(\mathbf{r}_{jk}) \hat{\sigma}_{22}^j \hat{\sigma}_{11}^k \right]$$

where  $\hat{H}_j = \Omega(\mathbf{r}_j) \hat{\sigma}_{21}^j / 2 + \text{H.c.}$  is single atom Hamiltonian with  $\hat{\sigma}_{\alpha\beta}^j = |\alpha^j\rangle\langle\beta^j|$  ( $\alpha, \beta = 1, 2$ ). Here Rabi frequency  $\Omega(\mathbf{r}_j) = \mathbf{d}_{21} \mathcal{E}(\mathbf{r}_j)$  depends on the slowly varying electric field  $\mathcal{E}(\mathbf{r})$  and dipole moment  $\mathbf{d}_{21}$  between the Rydberg and groundstate. To be concrete, Cs atoms will be considered in this work as the dipole moment is relatively large compared to other alkali atoms (see Supplementary Material (SM [41]) for details). Single-photon Rydberg excitation of ultracold Cs atoms has been demonstrated experimentally with nanosecond [42] and continuous lasers [43–46].

In addition to vdW and dipole-dipole interactions between Rydberg atoms, the attractive polarization interaction between electrons and groundstate atoms has been extensively studied previously [38, 39]. In ultracold gases, it leads to the formation of ultralong-range Rydberg molecules [47–50] and Rydberg polarons [51]. At high temperatures, it causes a spectra shift and inelastic collision due to mixing with other Rydberg states [39]. After compositing the shift with laser detuning, the inelastic collision is characterized by decay rate  $\gamma_{21}^c = \mathcal{N} v_T \sigma_{nP}$  [39] where  $v_T = \sqrt{2k_B T / M}$  is the thermal velocity ( $M$  mass of Cs atoms), and  $\sigma_{nP}$  the collisional cross-section [41]. As shown in Fig. 2a and b, the cross-section becomes larger with increasing principal quantum number,  $n$  and temperature,  $T$ . The decay rate moreover depends on atomic densities linearly. In high

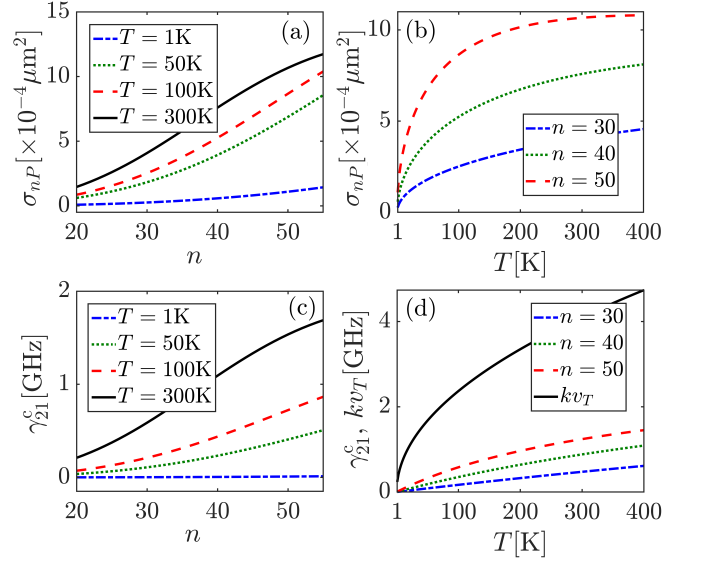


FIG. 2. (Color online) **Cross-section and collisional decay rate in Rydberg  $nP$  states.** The cross-section increases with higher  $n$  (a) and temperature (b). Collisional decay rates monotonically increases with  $n$  (c) and temperature (d). At room temperature, the rate is a few gigahertz for high Rydberg states that is comparable to the Doppler broadening. Here the atomic density is  $\mathcal{N} = 5 \times 10^{15} \text{cm}^{-3}$ , and s-wave scattering length of Cs atoms  $a_s \approx 21.7 a_B$  ( $a_B$  the Bohr radius).

density ( $> 10^{15} \text{cm}^{-3}$ ) gases, the decay, e.g.  $\gamma_{21}^c \sim 1$  gigahertz for  $T = 300$  K, can be comparable to the Doppler broadening (Fig. 2c-d).

Taking into account the inelastic collision, dynamics of the system is described by a set of coupled Maxwell-Bloch equations [52]. In the following, we will focus on pulse propagation along  $z$  direction while neglecting the diffraction, which is unimportant in short media. Applying the continuous density approximation, this yields the one dimensional (1D) Maxwell-Bloch equations,

$$i \frac{\partial}{\partial t} w(z) + \Omega(z) \rho_{12}(z) - \Omega^*(z) \rho_{21}(z) = 0, \quad (1a)$$

$$\left[ i \frac{\partial}{\partial t} + i \gamma_{21}^c - kv \right] \rho_{21}(z) + \frac{\Omega(z)}{2} w(z) - i \gamma_{21}^c f(v) R_{21}(z) - \mathcal{N}^{1/3} \int dz' dv' f(v') V_r(z' - z) \rho_{22,21}(z', z, t) = 0 \quad (1b)$$

$$i \left( \frac{\partial}{\partial z} + \frac{1}{c} \frac{\partial}{\partial t} \right) \Omega(z) + \frac{k}{2} \chi(z, t) \Omega(z) = 0, \quad (1c)$$

where  $\rho_{\alpha\beta}(z) = \langle \hat{\sigma}_{\alpha\beta}(z) \rangle$  is the mean value of operator  $\hat{\sigma}_{\alpha\beta}(z)$ , and  $w(z) = 1 - 2\rho_{22}(z)$  the population inversion.  $R_{21}(z) = \int dv \rho_{21}(z, v, t)$  and  $\chi(z) = 2\mathcal{N}(\mathbf{d}_{12})^2 \int dv f(v) \rho_{21}(z, v, t) / [\epsilon_0 \Omega(z)]$  are the integrated density and susceptibility [52], correspondingly.  $f(v) = 1/(\sqrt{\pi} v_T) \exp[-(v/v_T)^2]$  is the 1D Maxwell-Boltzmann velocity distribution. These equations couple to two-body correlation  $\rho_{\beta\alpha, \nu\mu}(z', z, t) \equiv \langle \hat{\sigma}_{\alpha\beta}(z', t) \hat{\sigma}_{\nu\mu}(z, t) \rangle$ , whose equation is cumbersome and therefore given in SM [41]. Note that finite Rydberg lifetimes (10 ~

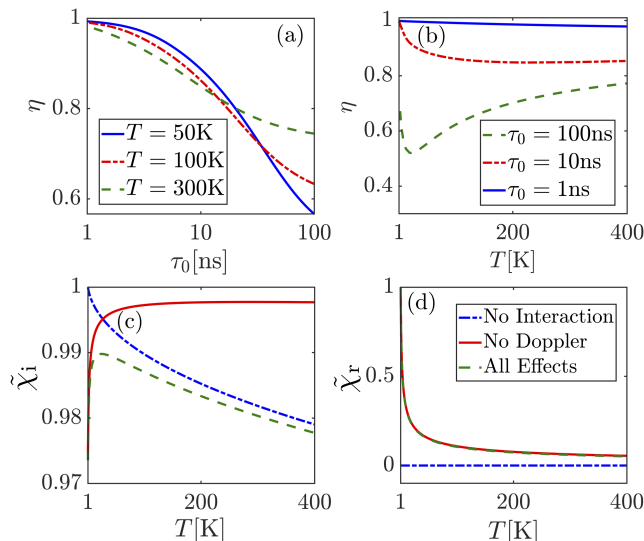


FIG. 3. (Color online) **Transmission of pulses.** The pulse duration (a) and temperature (b) of the medium affect the transmission. When  $\tau \sim 1$  ns,  $\eta \sim 1$  almost independent of the temperature. Notable absorption is found when  $\tau \gg 1$  ns (a). Transmission varies with temperature non-monotonically for very long pulses, e. g.  $\tau = 100$  ns in panel (b). The imaginary  $\tilde{\chi}_i = \text{Im}[\tilde{\chi}(T)]/\text{Im}[\tilde{\chi}_s]$  (c) and real part  $\tilde{\chi}_r = \text{Re}[\tilde{\chi}(T)]/\text{Re}[\tilde{\chi}_s]$  (d) of static susceptibility  $\tilde{\chi}(T)$  at temperature  $T$ , scaled with respect to  $\tilde{\chi}_s = \tilde{\chi}(T = 1\text{K})$ . The maximal  $\tilde{\chi}_i$  and maximal absorption for  $\tau = 100$  ns in (b) both locate around  $T = 10$  K. The absorption is suppressed at low and high temperatures, due to less Rydberg excitations (hence decay) caused by the Rydberg blockade and Doppler effect [53], respectively. The Rydberg interaction gives large real part  $\tilde{\chi}_r$ , which increases drastically at low temperatures. The legend in (c) and (d) is same. We consider Rydberg state  $|30P\rangle$  with lifetime  $27.79 \mu\text{s}$ ,  $L = 400 \mu\text{m}$  and  $\mathcal{N} = 5 \times 10^{15} \text{cm}^{-3}$ .

$100 \mu\text{s}$ ), which are much longer than typical timescales of the laser pulse, play no roles in the dynamics.

**Transmission of light pulses.**— We first study optical losses due to collisional decay and Doppler effects. The latter causes population trapping in Rydberg states, hence reducing the output intensity. To be concrete, we assume the pulse has a profile  $\Omega(z = 0) = \tilde{\Omega} \text{sech}[(t - t_0)/\tau]$  with  $\tilde{\Omega}$ ,  $t_0$  and  $\tau$  to be the amplitude, center and duration at the boundary  $z = 0$  (length of the medium  $L$ ). We want to emphasize that results in the following sections can be equally obtained by considering Gaussian pulses [41]. The Maxwell-Bloch equation is solved by a combination of the 4th order Runge-Kutter and Chebyshev spectral method [54]. Using the spatial-temporal solution we evaluate transmission at the output ( $z = L$ )  $\eta = \int_{-\infty}^{+\infty} dt |\Omega(L)|^2 / \int_{-\infty}^{+\infty} dt |\Omega(0)|^2$ .

For nanosecond pulses ( $\tau \sim 1$  ns), we find that transmission  $\eta \sim 1$ , indicating that the medium is almost transparent (Fig. 3a). An important feature is that transmission of nanosecond pulses is thermal robust. As shown in Fig. 3b, the reduction of  $\eta$  is marginal when the temperature increases from 1 K to 400 K. Note that both the decay rate and Doppler broadening become a

few gigahertz at 400 K (see Fig. 2c and d).

For long pulses, transmission becomes smaller at higher temperatures (Fig. 3b). When  $\tau \gg 10$  ns,  $\eta$  depends on the temperature non-trivially. For example,  $\eta$  decreases and then increases with increasing temperature for  $\tau = 100$  ns, due to the interplay between the Doppler and collisional effect. We can understand this dependence qualitatively by examining static susceptibility  $\tilde{\chi}(T)$  of infinitely long pulses, which is given analytically in SM [41]. By analyzing the imaginary part of  $\chi_s$  (Fig. 3c), the low transmission is caused by the collisional decay (Doppler effect) at low (high) temperatures. Moreover the real part of  $\tilde{\chi}$  becomes large at lower temperatures (Fig. 3d). It generates an optical phase when propagating in the medium.

**Rydberg-SIT of nanosecond pulses.**— Without atom-atom interactions, so-called *self-induced transparency* [37, 55] can occur if areas of nanosecond pulses fulfill  $\theta(z) = \int_{-\infty}^{\infty} \Omega(z, t) dt = 2K\pi$  ( $K$  is a integer), governed by the area theorem [55]. This is a nonlinear effect where the nonlinearity is rooted solely from high intensities. The intensity nonlinearity reshapes the pulse into a stable, bright soliton, i.e. no absorption or distortion. Furthermore, it reduces the group velocity ( $v_g \approx 2\varepsilon_0 |\Omega|^2 / (k\mathcal{N}d_{12}^2)$ ) but does not affect phases of the pulse [55].

The Rydberg nonlinearity changes SIT drastically. As an example, spatial-temporal distributions of the pulse for  $n = 30$  are shown in Fig. 4a-b. Different from conventional SIT, the profile is distorted when the input area  $\theta(0) = 2\pi$  (Fig. 4a). Our numerical simulations show that pulse shapes can be preserved if  $\theta(0) = 0.35\pi$  (Fig. 4b), leading to *Rydberg-SIT*. At the first instance, we can understand the formation of Rydberg-SIT at this optimal area from the transient dynamics of the atoms [37, 55]. The relevant quantity is the coherence  $\text{Im}(\rho_{21})$ , which is symmetric with respect to  $t_0$ , i.e. positive (negative) when  $t < t_0$  ( $t > t_0$ ). This means that the light is absorbed and then emitted coherently by atoms, where  $\rho_{22}, \rho_{21} \rightarrow 0$  when  $t \rightarrow +\infty$ . The dynamics is independent of  $z$ , i.e. the pulse translates in the medium. When the temperature increases from  $1 \mu\text{K}$  (Fig. 4c) to 300 K (Fig. 4d), we only see a marginal change of the pulse as the time average of  $\text{Im}(\rho_{21})$  is negligibly small.

To systematically study the pulse deformation, we define a fidelity  $F = \int_{-\infty}^{+\infty} dt |\Omega(L)\Omega(0)|^2 / \int_{-\infty}^{+\infty} dt |\Omega(L)|^2 \int_{-\infty}^{+\infty} dt |\Omega(0)|^2$ , which is 1 if the input and output pulse are identical. Through scanning the input areas in  $0 < \theta(0) \leq 2\pi$ , a single maximal fidelity appears at the optimal area. For different Rydberg states, the optimal area varies with  $n$ , see Fig. 4e. We also carried out large scale numerical calculations for  $20 \leq n \leq 50$ . It is found that the optimal area decreases monotonically with increasing  $n$ . At the same time, the corresponding fidelity is high, as shown in Fig. 4f.

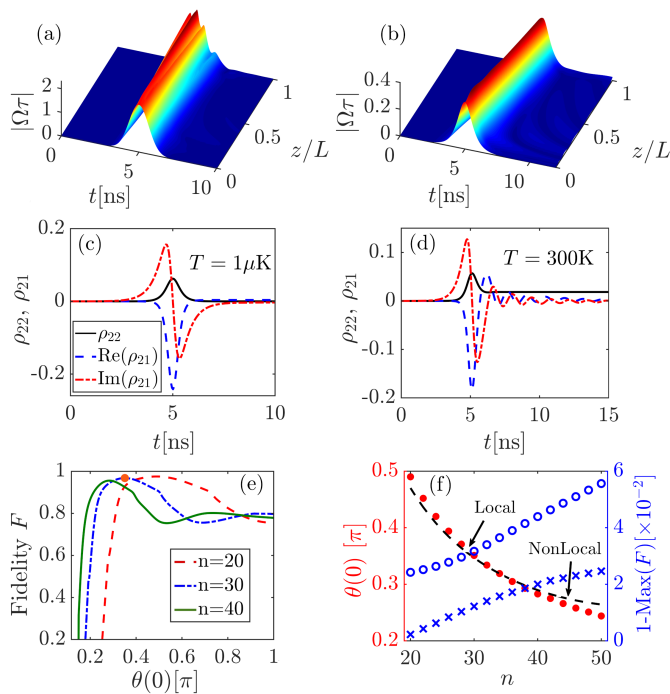


FIG. 4. (Color online) **Rydberg-SIT and the optimal area.** The pulse is distorted when  $\theta(0) = 2\pi$  (a). Robust propagation is found when  $\theta(0) = 0.35\pi$  (b), corresponding to Rydberg-SIT. The transient dynamics of atoms at  $T = 1 \mu\text{K}$  (c) and 300 K (d). Fully symmetric  $\text{Im}(\rho_{21})$  with respect to  $t_0$  leads to formation of Rydberg-SIT. Such dynamics is independent of  $z$ . (e) Fidelity  $F$  as a function of initial area  $\theta(0)$ . Maximal fidelities appear at optimal areas that depend on the Rydberg state. (f) Optimal area (filled circle) and corresponding fidelity at  $1 \mu\text{K}$  (star) and 300 K (empty circle). The MF result (dashed) agrees with the numerical calculation. In panel (a)-(d)  $n = 30$ . In (e)-(f), the pulse area is varied by changing  $\Omega$ . Other parameters  $t_0 = 5 \text{ ns}$ ,  $\tau = 1 \text{ ns}$ ,  $L = 400 \mu\text{m}$  and  $T = 300 \text{ K}$ .

**State-dependent optimal areas.**— In the remaining part, we will develop a mean field (MF) theory for the Bloch equation (BE) to understand the optimal area. Inspired by the transient dynamics (Fig. 4c-d), we will treat the MF equations in the time domain. To deal with the two-body interaction term in Eq. (1b), we will apply a local field approximation to the two-body correlations, i.e.  $\rho_{22,21}(z', z, t) \approx \rho_{22}(z, t)\rho_{21}(z, t)$  [8]. This is a valid approximation as the pulse is much longer than ranges of Rydberg interactions. With this approximation Eq. (1b) becomes,

$$\dot{\rho}_{21} \approx -\gamma_{21}^c [\rho_{21} - f(v)R_{21}] - i(kv + u\rho_{22})\rho_{21} - \frac{i\Omega w}{2}, \quad (2)$$

while other equations are not affected formally. Here  $u = 2\mathcal{N}^{1/3} \int_0^\infty dz V(z)$  is an effective detuning resulting from the Rydberg interaction. To avoid divergence in the integral, the vdW potential is modified at short distances to have soft-core shape,  $V(z) \approx C_6/(z^6 + z_m^6)$ , when atomic distances are smaller than the blockade radius  $z_m = (|C_6|/\tilde{\Omega})^{1/6}$  [2]. This allows us to analytically

evaluate the effective detuning  $\bar{u} = 4\pi\mathcal{N}^{1/3}C_6^{1/6}\tilde{\Omega}^{5/6}/3$ . This expression shows explicitly the dependence of  $u$  on the density, Rabi frequency and Rydberg state.

First, three different regimes of the coherence can be obtained approximately according to Eq. (2) depending on the ratio  $(kv_T + u)/\gamma_{21}^c$ , as shown in Fig. 1c. Fixing  $T$ , a Doppler broadening dominant region appears at low densities when  $kv_T > u \gg \gamma_{21}^c$ . For sufficiently high densities (dotted line,  $10kv_T = u$ ) Rydberg interactions overtakes the other two effects, i.e.  $u > kv_T \gg \gamma_{21}^c$ . This is the most interesting region where Rydberg-SIT can form. Further increasing densities (dashed line,  $kv_T + u = 100\gamma_{21}^c$ ), the collisional decay starts to kick in and causes losses when propagating in a medium.

In the next, we will find the optimal areas analytically in the interaction dominant region (i.e. neglecting terms involving  $kv_T$  and  $\gamma_{21}^c$ ). As the nonlinear Eq. (2) is still difficult to integrate with this approximation, we will apply the following ansatz solution  $\rho_{22} = A[1 - \cos \int_{-\infty}^t \Omega_0(t')dt']$  and  $\rho_{21} = -\frac{iB}{2} \cos \int_{-\infty}^t \Omega_0(t')dt' + C\rho_{22}$  where  $A$ ,  $B$ , and  $C$  are trial parameters. In the ansatz, we assume a Gaussian pulse  $\Omega_0(t) = \sqrt{2\pi} \exp(-t^2/2\tau^2)/\tau$  which ensure that  $\text{Im}[\rho_{21}]$  is symmetric with respect to the pulse center, and  $\rho_{12} = \rho_{22} = 0$  when  $t \rightarrow \infty$ . In the MF BE, the pulse has a Gaussian profile  $\Omega = \tilde{\theta} \exp(-t^2/2\tau^2)/\sqrt{2\pi}\tau$ , characterized by the unknown parameter  $\tilde{\theta}$ , which gives the area.

Substituting the ansatz to the effective BE, and using the initial conditions, the trial parameters and  $\tilde{\Omega}$  can be calculated explicitly (see SM [41] for details). This allows us to obtain a state dependent area,

$$\tilde{\theta} = \frac{2\pi}{u\tau} \left( \sqrt{2\pi u^2 \tau^2 + \pi^2} - \pi \right)^{\frac{1}{2}}, \quad (3)$$

which is a key result of the MF calculation. Eq. (3) shows  $\tilde{\theta} \rightarrow 2\pi$  when  $u \rightarrow 0$ , recovering the area theorem in non-interacting SIT [55]. Increasing  $u$ ,  $\tilde{\theta}$  decreases gradually. When compared with numerical data, an excellent agreement is found if  $n < 40$ . For  $n > 40$ , small deviations between the two calculations are noticed. The deviation attributes to the local field approximation, which does not capture full long-range features of the vdW interaction in highly excited Rydberg states.

**Conclusion and discussion.**— In this work, we study the propagation dynamics of short pulses in thermal, high-density Rydberg gases. We show strong dispersive optical nonlinearities can be achieved from low to high temperature. Due to the Rydberg nonlinearity, Rydberg-SIT can form in thermal atomic gases which is largely immune to the Doppler broadening and collisional decay. A key finding is that the optimal area of the Rydberg-SIT is reduced by the Rydberg atom interaction. We identify numerically and analytically optimal areas to realize a stable Rydberg-SIT regime.

This work opens exciting opportunities to study nonlinear optics and to implement quantum information

processing at nanosecond time scales with warm Rydberg gases. Beyond the current level scheme, one can also achieve strong Rydberg nonlinearities of short laser pulses using two-photon excitations. Due to large light-atom couplings, this allows us to study, for example simultons [56], in relatively low densities [41]. As the Rydberg nonlinearity can produce optical phases, one could implement quantum information applications, such as fast optical phase gates through cross-phase modulations (See SM [41] for demonstrations) [57–60], with Rydberg-SIT.

We thank insightful discussions with Thomas Gallagher, Igor Lesanovsky, Sebastian Slama, Lin Li, Jing Zhang, Jianming Zhao, Junmin Wang and Stephen Hogan. Z. B. and G. H. acknowledge National Science Foundation (NSF) (11904104, 11474099, 11174080, 11847221), The Shanghai Sailing Program (18YF1407100), China Postdoctoral Science Foundation (2017M620140), and the International Postdoctoral Exchange Fellowship Program (20180040). CSA acknowledges financial support from EPSRC Grant Ref. Nos. EP/R002061/1, EP/M014398/1, EP/S015973/1, EP/R035482/1 and EP/P012000/1, the EU RIA project ‘RYSQ’ project, EU-H2020-FETPROACT-2014 184 Grant No. 640378 (RYSQ) and DSTL. W. L. acknowledges support from the EPSRC through grant No. EP/R04340X/1 via the QuanterA project ERYQSenS, the Royal Society grant No. IEC\NSFC\181078, and the UKIERI-UGC Thematic Partnership (IND/CONT/G/16-17/73).

- 
- [1] D. Jaksch, J. I. Cirac, P. Zoller, S. L. Rolston, R. Ct, and M. D. Lukin, *Phys. Rev. Lett.* **85**, 2208 (2000).
- [2] M. D. Lukin, M. Fleischhauer, R. Ct, L. M. Duan, D. Jaksch, J. I. Cirac, and P. Zoller, *Phys. Rev. Lett.* **87**, 037901 (2001).
- [3] M. Saffman, T. G. Walker, and K. Mølmer, *Rev. Mod. Phys.* **82**, 2313 (2010).
- [4] J. D. Pritchard, D. Maxwell, A. Gauguet, K. J. Weatherill, M. P. A. Jones, and C. S. Adams, *Phys. Rev. Lett.* **105**, 193603 (2010).
- [5] D. Petrosyan, J. Otterbach, and M. Fleischhauer, *Phys. Rev. Lett.* **107**, 213601 (2011).
- [6] W. Li, D. Viscor, S. Hofferberth, and I. Lesanovsky, *Phys. Rev. Lett.* **112**, 243601 (2014).
- [7] O. Firstenberg, C. S. Adams, and S. Hofferberth, *J. Phys. B* **49**, 152003 (2016).
- [8] S. Sevinçli, N. Henkel, C. Ates, and T. Pohl, *Phys. Rev. Lett.* **107**, 153001 (2011).
- [9] Z. Bai and G. Huang, *Opt. Express* **24**, 4442 (2016).
- [10] Z. Bai, W. Li, and G. Huang, *Optica* **6**, 309 (2019).
- [11] A. V. Gorshkov, J. Otterbach, M. Fleischhauer, T. Pohl, and M. D. Lukin, *Phys. Rev. Lett.* **107**, 133602 (2011).
- [12] T. Peyronel, O. Firstenberg, Q.-Y. Liang, S. Hofferberth, A. V. Gorshkov, T. Pohl, M. D. Lukin, and V. Vuleti, *Nature* **488**, 57 (2012).
- [13] A. V. Gorshkov, R. Nath, and T. Pohl, *Phys. Rev. Lett.* **110**, 153601 (2013).
- [14] O. Firstenberg, T. Peyronel, Q.-Y. Liang, A. V. Gorshkov, M. D. Lukin, and V. Vuleti, *Nature* **502**, 71 (2013).
- [15] B. He, A. Sharypov, J. Sheng, C. Simon, and M. Xiao, *Phys. Rev. Lett.* **112**, 133606 (2014).
- [16] H. Busche, P. Huillery, S. W. Ball, T. Ilieva, M. P. A. Jones, and C. S. Adams, *Nat. Phys.* **13**, 655658 (2017).
- [17] Q.-Y. Liang, A. V. Venkatramani, S. H. Cantu, T. L. Nicholson, M. J. Gullans, A. V. Gorshkov, J. D. Thompson, C. Chin, M. D. Lukin, and V. Vuleti, *Science* **359**, 783 (2018).
- [18] D. Maxwell, D. J. Szwer, D. Paredes-Barato, H. Busche, J. D. Pritchard, A. Gauguet, K. J. Weatherill, M. P. A. Jones, and C. S. Adams, *Phys. Rev. Lett.* **110**, 103001 (2013).
- [19] L. Li and A. Kuzmich, *Nat. Commun.* **7**, 13618 (2016).
- [20] D. Tiarks, S. Schmidt, G. Rempe, and S. Drr, *Sci. Adv.* **2**, e1600036 (2016).
- [21] D. Tiarks, S. Schmidt-Eberle, T. Stolz, G. Rempe, and S. Drr, *Nat. Phys.* **15**, 124 (2019).
- [22] H. Gorniaczyk, C. Tresp, J. Schmidt, H. Fedder, and S. Hofferberth, *Phys. Rev. Lett.* **113**, 053601 (2014).
- [23] S. Baur, D. Tiarks, G. Rempe, and S. Dürr, *Phys. Rev. Lett.* **112**, 073901 (2014).
- [24] W. Li and I. Lesanovsky, *Phys. Rev. A* **92**, 043828 (2015).
- [25] D. Tiarks, S. Baur, K. Schneider, S. Dürr, and G. Rempe, *Phys. Rev. Lett.* **113**, 053602 (2014).
- [26] H. Gorniaczyk, C. Tresp, P. Bienias, A. Paris-Mandoki, W. Li, I. Mirgorodskiy, H. P. Bchler, I. Lesanovsky, and S. Hofferberth, *Nat. Commun.* **7**, 12480 (2016).
- [27] C. R. Murray and T. Pohl, *Phys. Rev. X* **7**, 031007 (2017).
- [28] C. Carr, R. Ritter, C. G. Wade, C. S. Adams, and K. J. Weatherill, *Phys. Rev. Lett.* **111**, 113901 (2013).
- [29] T. Baluktsian, B. Huber, R. Lw, and T. Pfau, *Phys. Rev. Lett.* **110**, 123001 (2013).
- [30] A. Urvoy, F. Ripka, I. Lesanovsky, D. Booth, J. Shaffer, T. Pfau, and R. Lw, *Phys. Rev. Lett.* **114**, 203002 (2015).
- [31] L. Zhang and J. Evers, *Phys. Rev. A* **94**, 033402 (2016).
- [32] F. Ripka, H. Kbler, R. Lw, and T. Pfau, *Science* **362**, 446 (2018).
- [33] S. Briaudeau, S. Saltiel, G. Nienhuis, D. Bloch, and M. Ducloy, *Phys. Rev. A* **57**, 3169(R) (1998).
- [34] M. Fichet, G. Dutier, A. Yarovitsky, P. Todorov, I. Hamdi, I. Maurin, S. Saltiel, D. Sarkisyan, M.-P. Gorza, D. Bloch, and M. Ducloy, *Europhys. Lett.* **77**, 54001 (2007).
- [35] D. Sarkisyan, T. Varzhapetyan, A. Sarkisyan, Y. Malakyan, A. Papoyan, A. Lezama, D. Bloch, and M. Ducloy, *Phys. Rev. A* **69**, 065802 (2004).
- [36] S. A. Moiseev and S. Krll, *Phys. Rev. Lett.* **87**, 173601 (2001).
- [37] S. L. McCall and E. L. Hahn, *Phys. Rev. Lett.* **18**, 908 (1967).
- [38] A. Omont, *J. Phys. France* **38**, 1343 (1977).
- [39] I. L. Beigman and V. S. Lebedev, *Phys. Rep.* **250**, 95 (1995).
- [40] Energy dependence of the electron-atom scattering is not important as average velocity of a Rydberg electron  $\sim v_0/n$  is far larger than the typical velocity of atoms at room-temperature.

- [41] See SupplementalMaterial for additional details about the model, mean field calculation, cross-phase modulation, and solitons, which includes Refs. [10](#), [11](#), [32](#), [39](#), [42](#), [52](#), [54](#), [61](#), and [62](#).
- [42] D. Tong, S. M. Farooqi, J. Stanojevic, S. Krishnan, Y. P. Zhang, R. Ct, E. E. Eyler, and P. L. Gould, [Phys. Rev. Lett.](#) **93**, 063001 (2004).
- [43] A. M. Hankin, Y.-Y. Jau, L. P. Parazzoli, C. W. Chou, D. J. Armstrong, A. J. Landahl, and G. W. Biedermann, [Phys. Rev. A](#) **89**, 033416 (2014).
- [44] Y.-Y. Jau, A. M. Hankin, T. Keating, I. H. Deutsch, and G. W. Biedermann, [Nat. Phys.](#) **12**, 71 (2016).
- [45] J. Wang, J. Bai, J. He, and J. Wang, [Opt. Express](#) **25**, 22510 (2017).
- [46] B. Li, M. Li, X. Jiang, J. Qian, X. Li, L. Liu, and Y. Wang, [Phy. Rev. A](#) **99**, 042502 (2019).
- [47] C. H. Greene, A. S. Dickinson, and H. R. Sadeghpour, [Phys. Rev. Lett.](#) **85**, 2458 (2000).
- [48] V. Bendkowsky, B. Butscher, J. Nipper, J. P. Shaffer, R. Lw, and T. Pfau, [Nature](#) **458**, 1005 (2009).
- [49] W. Li, T. Pohl, J. M. Rost, S. T. Rittenhouse, H. R. Sadeghpour, J. Nipper, B. Butscher, J. B. Balewski, V. Bendkowsky, R. Lw, and T. Pfau, [Science](#) **334**, 1110 (2011).
- [50] J. P. Shaffer, S. T. Rittenhouse, and H. R. Sadeghpour, [Nat. Commun.](#) **9**, 1 (2018).
- [51] F. Camargo, R. Schmidt, J. D. Whalen, R. Ding, G. Woehl, S. Yoshida, J. Burgdörfer, F. B. Dunning, H. R. Sadeghpour, E. Demler, and T. C. Killian, [Phys. Rev. Lett.](#) **120**, 083401 (2018).
- [52] O. Firstenberg, M. Shuker, R. Pugatch, D. R. Fredkin, N. Davidson, and A. Ron, [Phys. Rev. A](#) **77**, 043830 (2008).
- [53] A. Urvoy, C. Carr, R. Ritter, C. S. Adams, K. J. Weatherill, and R. Lw, [J. Phys. B](#) **46**, 245001 (2013).
- [54] J. P. Boyd, *Chebyshev and Fourier Spectral Methods: Second Revised Edition*, second edition ed. (Dover Publications).
- [55] G. L. Lamb, [Rev. Mod. Phys.](#) **43**, 99 (1971).
- [56] T. P. Ogden, K. A. Whittaker, J. Keaveney, S. A. Wrathmall, C. S. Adams, and R. M. Potvliege, [Phys. Rev. Lett.](#) **123**, 243604 (2019).
- [57] P. G. P. Agrawal, *Nonlinear Fiber Optics* (Academic Press, 2012).
- [58] M. N. Islam, [Opt. Lett.](#) **14**, 1257 (1989).
- [59] R. McLeod, K. Wagner, and S. Blair, [Phys. Rev. A](#) **52**, 3254 (1995).
- [60] B. A. Kochetov, I. Vasylieva, A. Butrym, and V. R. Tuz, [Phys. Rev. E](#) **99**, 052214 (2019).
- [61] V. Lebedev and V. Marchenko, [J. Exp. Theor.](#) **88**, 754 (1985).
- [62] D. A. Steck, “Alkali D Line Data,” .

# Supplementary information for

## Self-induced transparency in warm and strongly interacting Rydberg gases

Zhengyang Bai, Charles S. Adams, Guoxiang Huang and Weibin Li

This supplementary material gives further details on the analysis in the main text.

### A. THE PROPERTIES OF RYDBERG ATOMS

We shall first focus on the inelastic collision between Rydberg atom and groundstate atom. In dense and high temperature gases, the electron-atom collision mixes energetically neighboring Rydberg states. Effectively, the resulting *inelastic collision* causes decay of the Rydberg state with rate  $\gamma_{21}^c = \mathcal{N}v_T\sigma_{nP}$  [39] with  $\mathcal{N}$  and  $v_T = \sqrt{2k_B T/M}$  to be the density and thermal velocity ( $M$  mass of Cs atoms). The inelastic cross section  $\sigma_{nP}$  is [39, 61]

$$\sigma_{nP} = \sum_{n'} \frac{4v_0^2 a_s^2}{v_T^2 n'^3} \left[ \arctan\left(\frac{2}{\lambda}\right) - \frac{\lambda}{2} \ln\left(\frac{4 + \lambda^2}{\lambda^2}\right) \right],$$

where  $\lambda = |\delta_P + n' - n|v_0/(n^2 v_T)$  characterizes the inelasticity for the  $nP \rightarrow n'$  manifold transition.  $\delta_P$  and  $v_0 = \hbar/(ma_b)$  are the quantum defect and orbital velocity of the Rydberg electron (mass  $m$ ). The non-trivial dependence of the cross section on temperature and Rydberg states is shown in Fig. 2a and 2b in the main text. Note that cross sections in Rydberg states are smaller than that of the low-lying states (e.g.  $|6P\rangle$ ) [62], which could cause stronger decay.

The strength of the single photon transition depends on the transition dipole moment  $\mathbf{d}_{21}$  between the ground state and Rydberg state  $|nP_{3/2}\rangle$ . Fig. S1 show results for Rb and Cs atoms. The transition dipole for Cs is relatively large. We shall note that, to produce a Rydberg-SIT soliton, the input light intensity is needed to be intense due to the fact that the transition dipole moment  $\mathbf{d}_{21}$  between the ground state and Rydberg state is small, but it is still available with current experimental capabilities [42]. To be concrete, we can estimate the peak intensity  $I_{\max} = c\epsilon_0|E_{p\max}|^2/2 \simeq 0.08$  MW cm<sup>-2</sup> for generating such Rydberg-SIT soliton in Fig. 4d in the main text.

### B. THE DYNAMICS OF THE RYDBERG ATOM

In this section, we provide the theory of the many-body dynamics in warm and strongly interacting Rydberg gases. We will focus on the derivation of the hierarchy of equations for many-body correlators provided in the main text. We first treat the dynamics under the effective Hamiltonian in the Heisenberg picture. To this end we obtain the equation of motion for the expectation values  $\hat{\rho}$  from the corresponding operator Heisenberg equations. This yields the explicit expression of the Bloch equation,

$$i\frac{\partial}{\partial t}\rho_{11}(z) - i\Gamma\rho_{22}(z) - \mathbf{Re}[\Omega(z)\rho_{12}(z)] = 0, \quad (\text{S1a})$$

$$\frac{\partial}{\partial t}\rho_{22}(z) + \Gamma\rho_{22}(z) + \mathbf{Im}[\Omega(z)\rho_{12}(z)] = 0, \quad (\text{S1b})$$

$$\left[ i\frac{\partial}{\partial t} + i\gamma_{21}^c - kv \right] \rho_{21}(z) + \frac{\Omega(z)}{2}w(z) - i\gamma_{21}^c f(v)R_{21}(z) - \mathcal{N} \int d^3r' dv' f(v')V(r' - r)\rho_{22,21}(r', r, t) = 0, \quad (\text{S1c})$$

where  $\rho_{\alpha\beta}(z) = \langle \hat{\sigma}_{\alpha\beta}(z) \rangle$  is the mean value of operator  $\hat{\sigma}_{\alpha\beta}(z)$ , and these equations couple to two-body correlation  $\rho_{\beta\alpha,\nu\mu}(z', z, t) \equiv \langle \hat{\sigma}_{\alpha\beta}(z', t)\hat{\sigma}_{\nu\mu}(z, t) \rangle$ , which are contributed from the interaction between Rydberg atoms.  $\Gamma$  is the spontaneous decay rate in Rydberg state, which is small quantity, i.e.  $\Gamma \ll \Omega, \gamma_{21}^c, kv_T$ .

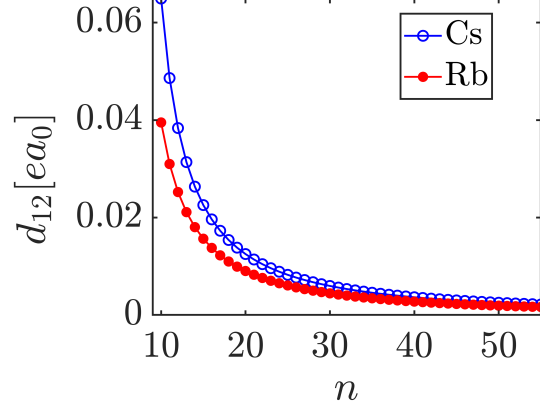


FIG. S1. (Color online) The transition dipole moment  $\mathbf{d}_{21}$  between the ground state and Rydberg state  $|nP_{3/2}\rangle$  for Rb and Cs atom.

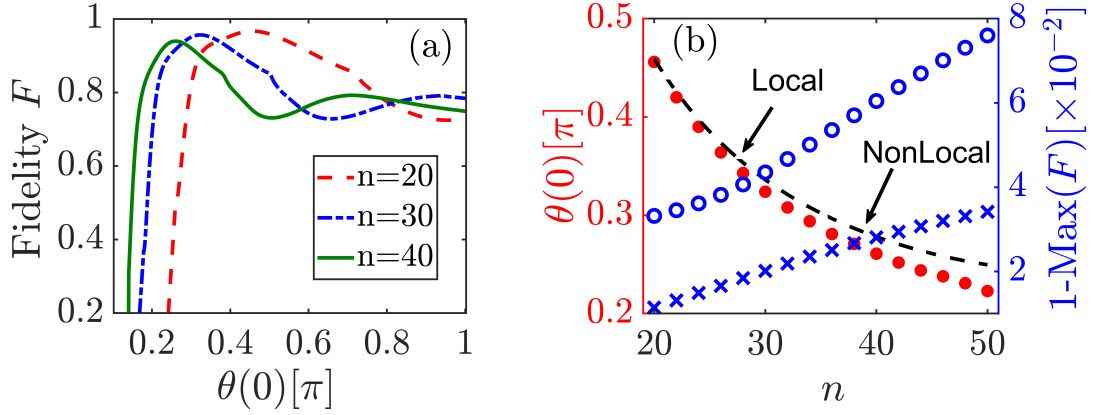


FIG. S2. (Color online) The optimal area for light pulse with Gaussian profile. (a) Fidelity  $F$  as a function of initial area  $\theta(0)$ . Maximal fidelities appear at areas depending on the Rydberg states. The pulse area is varied by changing the amplitude of  $\Omega$ . (b) The optimal area (circle) and corresponding output fidelity (square) of different Rydberg states. The dashed line is the optimal area predicted by Eq. (3) in the main text, which agrees with our numerical data. The parameters used here are same as the results shown in Fig. 4 in the main text.

From equation (S1c), we see that to solve the one-body correlators  $\rho_{\beta\alpha}(\mathbf{r}, v, t) \equiv \langle \hat{\sigma}_{\alpha\beta}(\mathbf{r}, t) \rangle$ , one needs to solve the equations of motion for the two-body correlators  $\rho_{\beta\alpha, \nu\mu}(\mathbf{r}', \mathbf{r}, v', v, t) \equiv \langle \hat{\sigma}_{\alpha\beta}(\mathbf{r}', v', t) \hat{\sigma}_{\mu\nu}(\mathbf{r}, v, t) \rangle$ , where a complete list of the equations of motion for the two-body density matrix (correlator) elements of the system is given by

$$\left( i \frac{\partial}{\partial t} + d_{21}(v') + d_{21}(v) - V_r(\mathbf{r}' - \mathbf{r}) \right) \rho_{21,21} - 2\Omega_p \rho_{22,21} + \Omega_p \rho_{21} = 0, \quad (\text{S2a})$$

$$\left( i \frac{\partial}{\partial t} + d_{21}(v) + d_{12}(v') \right) \rho_{21,12} - \Omega_p \rho_{22,12} + \Omega_p^* \rho_{21,22} + \frac{\Omega_p}{2} \rho_{12} - \frac{\Omega_p^*}{2} \rho_{21} = 0, \quad (\text{S2b})$$

$$\left( i \frac{\partial}{\partial t} + i\Gamma_{12} + d_{21}(v) - V_r(\mathbf{r}' - \mathbf{r}) \right) \rho_{22,21} + \frac{\Omega_p}{2} \rho_{12,21} - \frac{\Omega_p^*}{2} \rho_{21,21} - \Omega_p \rho_{22,22} + \frac{\Omega_p}{2} \rho_{22} = 0, \quad (\text{S2c})$$

$$\left( i \frac{\partial}{\partial t} + 2i\Gamma_{12} \right) \rho_{22,22} + \Omega_p \rho_{12,22} - \Omega_p^* \rho_{21,22} = 0, \quad (\text{S2d})$$

where  $d_{21}(v) = i\gamma_{21}^c - k_p v$  and  $d_{12}(v) = i\gamma_{21}^c + k_p v$ . Here the motion of equations are closed for one-body and two-body correlations and their number becomes finite, due to the fact that higher-order many-body correlators involved in the hierarchy play no significant role and hence can be truncated in our calculation [10].

Focusing on light propagation in  $z$ -axis (i.e. neglecting diffraction), the propagation of the light pulse field is

governed by one dimensional (1D) Maxwell equation,

$$i \left( \frac{\partial}{\partial z} + \frac{1}{c} \frac{\partial}{\partial t} \right) \Omega(z) + \frac{k}{2} \chi(z, t) \Omega(z) = 0, \quad (\text{S3})$$

where  $\chi(z) = 2\mathcal{N}(\mathbf{d}_{12})^2 \int dv f(v) \rho_{21}(z, v, t) / [\varepsilon_0 \Omega(z)]$  are the integrated density and temperature dependent susceptibility [52], correspondingly.  $f(v) = 1/(\sqrt{\pi}v_T) \exp[-(v/v_T)^2]$  is the 1D Maxwell-Boltzmann velocity distribution. In the main text, we use a combination of the 4th order Runge-Kutter and Chebyshev spectral method to solve the coupled Maxwell-Bloch equation [54].

In the main text, we have already showed numerical results when the profile is described by the sech function. Without loss of generality, we show the results for the Gaussian profile in Fig. S2. We can see that similar optimal areas can be found in the numerical calculations. This also justifies that it is a good approximation to use the Gaussian profile in the mean field calculation.

### C. STEADY-STATE SUSCEPTIBILITY

In this section, we shall give a static picture to explain absorption of long pulses. To realize atom-atom interaction, we assume that a gate excitation is stored in another Rydberg state  $|3\rangle = |n'P\rangle$  [11]. After preparing the initial state, a source field is sent to the medium and collide with the gate Rydberg excitation. The interaction between atoms in state  $|2\rangle$  and  $|3\rangle$  reads  $V_d(z_{jk}) = -C_6^d/|z_j - z_k|^6$  ( $C_6^d$  dispersion coefficient of the interstate interaction). To obtain an analytical expression of coherence  $\rho_{21}$ , we assume that the light is a continuous wave, thus optical Bloch equation can be easily written in the frequency space,

$$-i\omega \tilde{\rho}_{22}(z) + \Gamma \tilde{\rho}_{22}(z) + \mathbf{Im} [\Omega(z) \tilde{\rho}_{12}(z)] = 0, \quad (\text{S4a})$$

$$(\omega + i\gamma_{21}^c - V_d(z) - kv) \tilde{\rho}_{21}(z) - \Omega(z) \tilde{\rho}_{22}(z) + \Omega(z)/2 = 0, \quad (\text{S4b})$$

where  $\rho_{\alpha\beta} = \int d\omega \tilde{\rho}_{\alpha\beta} \exp(-i\omega t)$ . Thus, it is easy for us to derive the coherence  $\rho_{21}$  to the lowest order approximation of the frequency,

$$\rho_{21} = \frac{(i\gamma_{21}^c + V_d + kv)\Gamma\Omega}{2[\gamma_{21}^c(\Omega^2 + \gamma_{21}^c\Gamma) + \Gamma(V_d + kv)^2]}, \quad (\text{S5})$$

After substituting Eq. (S5) into the Maxwell Equation (S3), and then integrate it, the coupled Bloch-Maxwell equation can be solved,

$$\Omega(z) = \Omega(0) \exp(i\phi - \alpha), \quad (\text{S6a})$$

$$\tilde{\chi} = \frac{\mathcal{N}\mathbf{d}_{12}^2}{2\varepsilon_0} \int f(v) \frac{(i\gamma_{21}^c + V_d + kv)\Gamma}{\gamma_{21}^c(\Omega^2 + \gamma_{21}^c\Gamma) + \Gamma(V_d + kv)^2} dv, \quad (\text{S6b})$$

where  $\phi = k \int_0^L \text{Re}(\tilde{\chi}) dz$  characters a picked-up phase by gate atom and  $\alpha = k \int_0^L \text{Im}(\tilde{\chi}) dz$  contributes to the optical absorption. Fig. 2c in the main text shows the imaginary of  $\tilde{\chi}$ , and one can see that the absorption is suppressed at low and high temperatures, due to less Rydberg excitations (hence decay) caused by the Rydberg blockade and Doppler effect, respectively.

For nanosecond pulses ( $\tau \sim 1$  ns), we find that transmission  $\eta \sim 1$ , indicating that the medium is almost transparency (see Fig. 2a in the main text). Moreover, the real part of  $\tilde{\chi}$  is nonzero (see Fig. 3d in the main text), and it could implement quantum information applications, such as fast optical phase gates through cross-phase modulations.

### D. MEAN FIELD CALCULATION

In the MF approximation, the Doppler Broadening and collisional decay terms are neglected. For Rydberg-SIT, the pulse is translationally invariant in the medium, we can neglect the spatial dependence in the BE. This gives the following MF equation,

$$\dot{w} = i\Omega(\rho_{21} - \rho_{12}), \quad (\text{S7})$$

$$\dot{\rho}_{12} \approx \frac{i}{2}\Omega w + \frac{i u}{2}(1-w)\rho_{12}, \quad (\text{S8})$$

$$\dot{\rho}_{21} \approx -\frac{i}{2}\Omega w - \frac{i u}{2}(1-w)\rho_{21}, \quad (\text{S9})$$

where the pulse is given by  $\Omega = \tilde{\theta} \exp(-t^2/2\tau^2) / \sqrt{2\pi}\tau$ . We can easily show that the area of the pulse is  $\tilde{\theta}$ . To be concrete, we have assumed that the MF equation is dealt at  $z = 0$ , such that the phase of the pulse is negligible, i.e.  $\Omega$  is a real function.

For convenience, we define two new variables for the coherence,  $s = \rho_{12} + \rho_{21}$  and  $h = \rho_{12} - \rho_{21}$ . The MF equations can be rewritten as

$$\dot{w} = i\Omega h, \quad (\text{S10})$$

$$\dot{s} = \frac{i u}{2}(1-w)h, \quad (\text{S11})$$

$$\dot{h} = i\Omega w + \frac{i u}{2}(1-w)s. \quad (\text{S12})$$

We will solve the MF equations with the ansatz

$$\rho_{22} = A[1 - \cos \int_{-\infty}^t \Omega_0(t') dt'], \quad (\text{S13})$$

$$\rho_{21} = -\frac{iB}{2} \cos \int_{-\infty}^t \Omega_0(t') dt' + C\rho_{22}, \quad (\text{S14})$$

where  $A$ ,  $B$ , and  $C$  are trial parameters. In the ansatz, we choose a Gaussian pulse  $\Omega_0(t) = \theta_0 \exp(-t^2/2\tau^2) / \tau\sqrt{2\pi}$ , whose area is  $\theta_0 = 2\pi$ .

To solve the MF equation sequentially, we first substituting the ansatz into Eq. (S10) and find

$$\dot{w} = -2A\Omega_0 \sin F(t) = -B\Omega \sin F(t), \quad (\text{S15})$$

where we have defined,

$$F(t) = \int_{-\infty}^t \Omega_0 dt' = \frac{\theta_0}{2} \left[ 1 + \text{Erf} \left( \frac{t}{\sqrt{2}\tau} \right) \right]. \quad (\text{S16})$$

One can prove that  $\cos F(t) = -1$  when  $t = 0$  and  $\cos F(t) = 1$  when  $t = \pm\infty$ . If we cancel the time-dependent terms on both sides in the above equation, this gives a relation between  $A$  and  $B$ ,

$$A = \frac{\tilde{\theta}}{2\theta_0} B. \quad (\text{S17})$$

From Eq. (S11) and  $\dot{s} = 4AC\Omega_0 \sin F(t)$ , we can get a time-dependent equation

$$4AC\Omega_0 = -uAB[1 - \cos F(t)]. \quad (\text{S18})$$

We consider  $t = 0$  in this equation. Using  $\cos F(0) = -1$  and  $A \neq 0$ , we obtain a relation between  $B$  and  $C$ ,

$$C = \frac{\sqrt{2\pi}u\tau}{2\theta_0} B. \quad (\text{S19})$$

Carrying out same procedure for Eq. (S12) and using  $\dot{h} = iB\Omega_0 \cos F(t)$ , we obtain an equation

$$B\Omega_0 \cos F(t) = \Omega[1 - 2A(1 - \cos F(t))] + 4uA^2C(1 - \cos F(t))^2. \quad (\text{S20})$$

At  $t = +\infty$ , we can apply  $\cos F(t) = 1$  and  $\lim_{t \rightarrow \infty} \Omega/\Omega_0 = \tilde{\theta}/\theta_0$ . This allows us to derive

$$B = \frac{\tilde{\theta}}{\theta_0}. \quad (\text{S21})$$

To solve the parameters, we again use Eq. (S20) and consider  $t = 0$ . This leads to equation

$$B\theta_0 + \tilde{\theta}(1 - 4A) + 16u\tau CA^2 = 0. \quad (\text{S22})$$

Substituting Eqns. (S17), (S21) and (S19) into this equation, this gives an equation for  $\tilde{\theta}$

$$\frac{u^2\tau^2}{\theta_0^5} \tilde{\theta}^4 + \frac{1}{\theta_0^2} \tilde{\theta}^2 - 1 = 0. \quad (\text{S23})$$

Solving this equation, we get the solution to the area,

$$\tilde{\theta} = \frac{2\pi}{u\tau} \left( \sqrt{2\pi u^2 \tau^2 + \pi^2} - \pi \right)^{\frac{1}{2}}, \quad (\text{S24})$$

which was used to compare against numerical data in the main text. With the explicit solution, parameters  $A$ ,  $B$ , and  $C$  can also be solved.

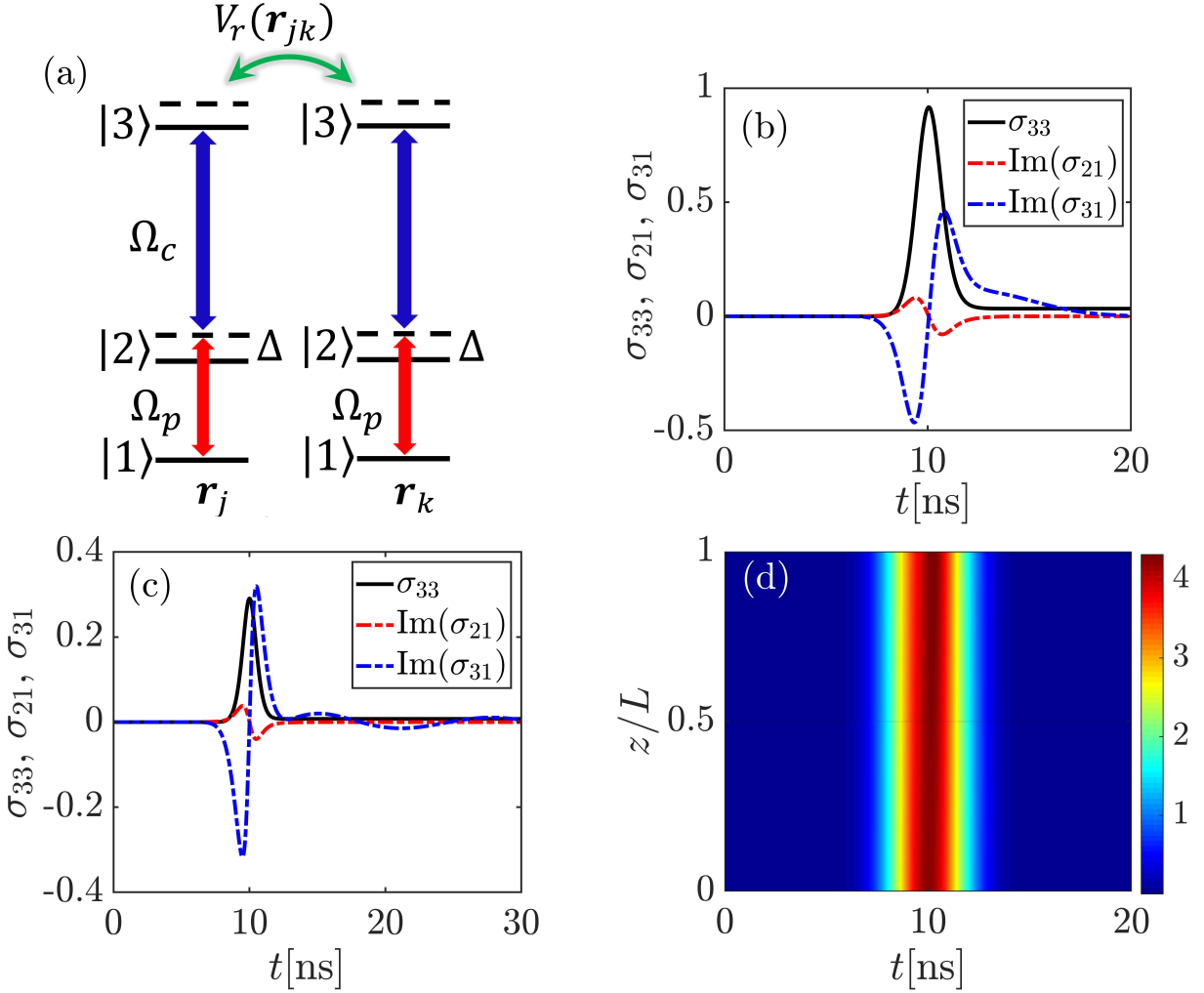


FIG. S3. (Color online) (a) The three level Ladder-type excitation scheme, where a weak probe field couples the ground state  $|1\rangle$  and the intermediate state  $|2\rangle$  (with Rabi frequency  $\Omega_p$ ), and a coupling field couples  $|2\rangle$  and the Rydberg state  $|3\rangle$  (with Rabi frequency  $\Omega_c$ ), respectively.  $\Delta$  are one-photon detunings, and the probe and coupling laser fields counter-propagate in the Rydberg gas. Rydberg atoms interact through the van der Waals interaction  $V_r(\mathbf{r}_{jk})$ . (b) The excitation  $\rho_{33}$  and the imaginary part of atomic coherence  $\rho_{21}$  and  $\rho_{31}$  as a function  $t$  for temperature  $T = 300\text{K}$  and initial effective pulse area  $\theta_m(z=0) = 2\pi$  [correspond to  $\theta_p(z=0) = 13.8\pi$ ]. In this case, atom-atom interaction is not taken into consideration. (c) The excitation  $\rho_{33}$  and the imaginary part of atomic coherence  $\rho_{21}$  and  $\rho_{31}$  as a function  $t$  for temperature  $T = 300\text{K}$ ,  $n = 30$ , and initial effective pulse area  $\theta_m(z=0) = 0.95\pi$  [correspond to  $\theta_p(z=0) = 9.5\pi$ ]. A large shift for probe pulse area can be observed with strong atom-atom interaction. (d) The probe pulse profile is robust when  $\theta_p(z=0) = 9.5\pi$  during the propagation. The parameters used here are given in Eq. (S28).

### E. SIT IN THREE-LEVEL MODEL

In the main text, Rydberg-SIT in two level model is shown to give an intuitive understanding of state-dependent optimal pulse area. However, due to the weak transition dipole between Rydberg state and ground state, very dense atomic density and long medium size are desired to observe the state-dependent pulse area. This could also be a challenging for conducting the experiment. In this section, we shall show a modified-SIT in the Rydberg-dressed three-level system and present qualitatively similar predictions for both models, and demonstrate that three-level system are more observable under current experimental conditions. See Sec. E for the demonstration of the optical phase gate.

We start to consider is a thermal, lifetime-broadened three-level atomic gas with a ladder-type EIT configuration, as illustrated in Fig. S3a. The electric field of the pulsed laser fields interacting with the atomic gas reads  $\mathbf{E}(\mathbf{r}, t) = \mathbf{E}_p + \mathbf{E}_c = \sum_{l=p,c} \mathbf{e}_l \mathcal{E}_l \exp[i(\mathbf{k}_l \cdot \mathbf{r} - \omega_l t)] + \text{c.c.}$ , where  $\mathbf{e}_l$  ( $\mathbf{k}_l$ ) is the unit polarization vector (wavevector) of the electric-field component with the envelope with  $\mathcal{E}_l$  ( $l = p, c$ ). The probe and coupling laser fields counter-propagate in the Rydberg gas. Here, a probe laser field  $\mathbf{E}_p$  (with wave number  $k_p = 2\pi/\lambda_p$  and Rabi frequency  $\Omega_p$ ) couples

to the transition between ground state  $|1\rangle$  and intermediate state  $|2\rangle$ ; a coupling laser field  $\mathbf{E}_c$  (with wave number  $k_c = 2\pi/\lambda_c$ , and Rabi frequency  $\Omega_c$ ) couples to the transition between intermediate state  $|2\rangle$  and Rydberg state  $|3\rangle$ .  $\Delta = \omega_p - (\omega_2 - \omega_1)$  is the one-photon detuning frequencies; By including the interatomic coupling between the excited Rydberg atoms, the Hamiltonian in the interaction picture and rotating-wave approximation reads ( $\hbar \equiv 1$ ),

$$\hat{H} = \sum_{j=1}^N \left[ \Delta_2 \hat{\sigma}_{22}^j + \Delta_3 \hat{\sigma}_{33}^j + \frac{1}{2} \tilde{\Omega}_p(\mathbf{r}_j) \hat{\sigma}_{21}^j + \frac{1}{2} \tilde{\Omega}_c(\mathbf{r}_j) \hat{\sigma}_{23}^j + \text{H.c.} \right] + \sum_{k \neq j}^N \left[ \frac{1}{2} V_r(\mathbf{r}_{jk}) \hat{\sigma}_{33}^j \hat{\sigma}_{33}^k \right], \quad (\text{S25})$$

where  $\hat{\sigma}_{\alpha\beta}^j = |\alpha^j\rangle\langle\beta^j|$ ,  $\tilde{\Omega}_{p(c)}(\mathbf{r}_j) = e^{ik_{p(c)}z_j} \Omega_{p(c)}(\mathbf{r}_j)$ , and  $\Omega_{p(c)}(\mathbf{r}_j) = \mathbf{d}_{21} \mathcal{E}_{p(c)}(\mathbf{r}_j)$  is the slowly varying Rabi frequency. The effective one- and two-photon detunings are given as  $\Delta_2 = \Delta - k_p v$  and  $\Delta_3 = (k_c - k_p)v$  respectively. The exactly dissipative dynamics of the laser-driven system with the Hamiltonian  $\hat{H}$  can be described by the master equation

$$\dot{\rho} = -i[\hat{H}, \rho] + D_1(\rho) + D_2(\rho), \quad (\text{S26})$$

where the Lindblad operators are defined as  $D_1(\rho) = \Gamma_{12} \sum_{j=1}^N \left( \hat{\sigma}_{12}^j \rho \hat{\sigma}_{21}^j - \{\hat{\sigma}_{22}^j, \rho\}/2 \right)$  and  $D_2(\rho) = \Gamma_{23} \sum_{j=1}^N \left( \hat{\sigma}_{23}^j \rho \hat{\sigma}_{32}^j - \{\hat{\sigma}_{33}^j, \rho\}/2 \right)$ . Besides, considering light propagation in  $z$ -axis (i.e. neglecting diffraction), the dynamics of the probe and coupling fields are described by the Maxwell equation, which under slowly varying amplitude approximation is reduced into

$$i \left( \frac{\partial}{\partial z} + \frac{1}{c} \frac{\partial}{\partial t} \right) \Omega_p(z) + \frac{k}{2} \chi_p(z, t) \Omega_p(z) = 0, \quad (\text{S27a})$$

$$i \left( \frac{\partial}{\partial z} + \frac{1}{c} \frac{\partial}{\partial t} \right) \Omega_c(z) + \frac{k}{2} \chi_c(z, t) \Omega_c(z) = 0, \quad (\text{S27b})$$

where  $\chi_{p(c)}(z) = 2\mathcal{N}_a [\mathbf{d}_{12(23)}]^2 \int dv f(v) \rho_{21(32)}(z, v, t) / [\varepsilon_0 \Omega_{p(c)}(z)]$  is the temperature dependent susceptibilities for probe and coupling fields. Here  $\mathbf{d}_{12}$  is the dipole moment between the ground state  $|1\rangle$  and the intermediate state  $|2\rangle$ , and  $\mathbf{d}_{23}$  is the dipole moment between the intermediate state  $|2\rangle$  and the Rydberg state  $|3\rangle$ .  $\mathbf{d}_{12}$  has two order magnitude larger than  $\mathbf{d}_{23}$ , thus the evolution of the probe field are more observable in the experiments.

Here we can take  $^{87}\text{Rb}$  atomic gas as a realistic candidate for our theoretical model described above. The energy-levels shown in Fig. S3a are selected to be  $|1\rangle = |5S_{1/2}\rangle$ ,  $|2\rangle = |5P_{3/2}\rangle$ , and  $|3\rangle = |nS_{1/2}\rangle$ . To simulate the propagation of the probe field, other system parameters are given by,

$$\begin{aligned} \mathcal{N}_a &= 1 \times 10^{13} \text{ cm}^{-3}, \quad \Delta = 60 \text{ GHz}, \quad L = 200 \text{ } \mu\text{m}, \\ n &= 30, \quad T = 300 \text{ K}, \quad \tau_0 = 1 \text{ ns}, \end{aligned} \quad (\text{S28})$$

For large one-photon detuning  $\Delta$ , three-level system can be equivalent to effective two-level system, and the effective two-level Rabi frequency  $\Omega \simeq \Omega_p \Omega_c / (2\Delta)$ . To be concrete, we can adopt effective Rabi frequency  $\Omega(t) = \Omega_m \exp(-t^2/2\tau_0^2) / \sqrt{2\pi}$ , in this case, the area of the effective pulse is given by  $\theta_m = \int_{-\infty}^{\infty} \Omega(t') dt' = \Omega_m \tau_0$ . Without loss of generality, we can assume  $\Omega_p = \Omega_c$ , thus the probe field have the form  $\Omega_p = \sqrt{2\Delta\Omega_m / \sqrt{2\pi}} \exp(-t^2/4\tau_0^2)$ , with probe pulse area  $\theta_p = \int_{-\infty}^{\infty} \Omega_p(t') dt' = \sqrt{2\sqrt{2\pi}\Delta\Omega_m} \tau_0$ . For no interaction case, the initial condition  $\theta_m(z=0) = 2\pi$  [correspond to  $\theta_p(z=0) = 13.8\pi$ ], one finds that the first part of a  $2\pi$  pulse transfers its energy to the atoms [see  $\text{Im}[\rho_{21}(t < 10)] > 0$  in Fig. S3b], and as long as coherence is maintained, this energy is then re-emitted in phase back into the second half of the pulse [see  $\text{Im}[\rho_{21}(t > 10)] < 0$  in Fig. S3b]. For Rydberg-dressed three-level system (i.e., we select Rydberg state  $|3\rangle = |30S_{1/2}\rangle$  here), atomic coherence and population shows the similar profile by adopting the modified effective pulse area  $\theta_m(z=0) = 0.95\pi$  [correspond to  $\theta_p(z=0) = 9.5\pi$ , see Fig. S3c]. Shown in Fig. S3d, one sees that an intense, short pulse can render an opaque medium completely transparency and propagate very stable. Moreover, we shall note that the modified probe pulse area in the three-level system is amplified by the factor  $\sqrt{2\sqrt{2\pi}\Delta/\Omega_m}$ , which might be easier to observe in the experiments.

With Rydberg-dressed three-level system, one could implement quantum information applications, such as optical phase gates through cross-phase modulations in a robust propagation. Here we just show a simple example, where a conditional phase gate can be realized in a short medium by using additionally Rydberg state  $|4\rangle = |n'S\rangle$ . To implement the phase gate, a gate excitation is stored in state  $|4\rangle$  via a short  $\pi$  pulse. Immediately after preparing the initial state, nanosecond pulses (control and probe field) are sent to the medium and collide with the gate

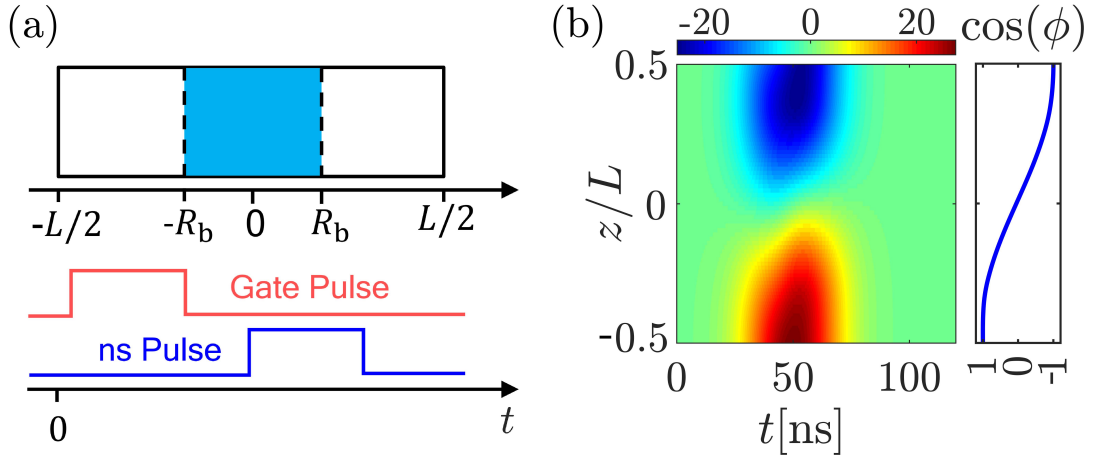


FIG. S4. (Color online) **Conditional phase induced by the cross-phase modulation.** (a) The pulse sequence: to implement the phase gate, a gate excitation is stored in state  $|4\rangle$  via a short  $\pi$  pulse. Immediately after preparing the initial state, nanosecond pulse (probe and control fields) are sent to the medium and collide with the gate Rydberg excitation. (b) Evolution of the real part  $\text{Re}(\Omega_p)$  of the probe pulse. An uniform phase accumulated to  $\pi$  can be observed when interacting with the gate excitation. We consider length  $L = 14\mu\text{m}$ , temperature  $T = 300\text{K}$ ,  $n = 70$ ,  $\tau_0 = 10$  ns, and atomic density  $\mathcal{N} = 2.4 \times 10^{15} \text{cm}^{-3}$  here.

Rydberg excitation (see Fig. S4a for the pulse sequence). To be concrete, we consider two Rydberg states with principal quantum number  $n =$  (gate excitation) and  $n' =$  (source excitation). The gate laser has a waist  $2R_b$  with  $R_b = |C_6^d/\Omega|^{1/6}$ . It perpendicularly passes through the medium in the middle (Fig. S4a), such that the gate excitation locates in  $-R_b < z < R_b$ . To mitigate thermal effects, both the gate and source laser have 10 ns duration. Ideally the gate excitation forms a collective state  $|G\rangle = 1/\sqrt{N} \sum_j |1 \cdots 4_j \cdots 1\rangle$ . Through solving the respective Bloch equation, we find the excitation probability of the gate atom is typically smaller than 1 due to thermal effects. This is taken into account in calculating the gate performance. When the source pulse propagates in the medium, it accumulates a  $\pi$  phase when interacting with gate atoms (see Fig. S4b). By manipulating the ratio between the control and probe fields, strong photon-photon interactions in nanosecond regime might be expected in a Rydberg-dressed SIT system, and we will address this interesting and vital topic elsewhere.